

Janus Skyrmion: Interfacial Quasiparticle with Two-Faced Helicity

Xichao Zhang,^{1,*} Rui Zhang,² Qiming Shao,³ Yan Zhou,⁴
Charles Reichhardt,⁵ Cynthia J. O. Reichhardt,⁵ and Masahito Mochizuki^{1,†}

¹*Department of Applied Physics, Waseda University, Okubo, Shinjuku-ku, Tokyo 169-8555, Japan*

²*Department of Physics, The Hong Kong University of Science and Technology, Clear Water Bay, Kowloon, Hong Kong, China*

³*Department of Electronic and Computer Engineering, The Hong Kong University of Science and Technology, Clear Water Bay, Kowloon, Hong Kong, China*

⁴*Guangdong Basic Research Center of Excellence for Aggregate Science, School of Science and Engineering, The Chinese University of Hong Kong, Shenzhen, Guangdong 518172, China*

⁵*Theoretical Division and Center for Nonlinear Studies, Los Alamos National Laboratory, Los Alamos, New Mexico 87545, USA*

(Dated: September 9, 2025)

Janus particles are functional particles with at least two surfaces showing asymmetric properties. We show at the interface between two magnetic regions with different antisymmetric exchange interactions, a new species of topological quasiparticles can emerge, in which different helicity structures can coexist. We name such an interfacial quasiparticle a “Janus skyrmion”, in analogy to the Janus particle. As the Janus skyrmion shows helicity asymmetry, its size could vary with both the in-plane and out-of-plane magnetic fields. A vertical spin current could drive the Janus skyrmion into one-dimensional motion along the interface without showing the skyrmion Hall effect, at a speed which depends on both the spin polarization angle and current density. Thermal fluctuations could also lead to one-dimensional random walk of a Brownian Janus skyrmion. This work uncovers unique dynamics of interfacial quasiparticles with exotic helicity structures, which may be realized in interface-engineered magnetic layers.

Introduction.—In chiral magnetic materials, antisymmetric exchange interactions, that is, Dzyaloshinskii-Moriya (DM) interactions [1, 2], could give rise to localized spin textures with nontrivial topology [3–12], which are usually treated as quasiparticles as they have well-defined shape, nanoscale size, and good mobility [11]. These magnetic quasiparticles could be dynamically manipulated by external drives, such as spin currents [13–18], and are considered to be next-generation information carriers for both conventional and quantum devices [19–26]. Although different magnetic quasiparticles may carry identical integer topological charge [8, 12], which is described by $Q = \frac{1}{4\pi} \int \mathbf{m} \cdot (\frac{\partial \mathbf{m}}{\partial x} \times \frac{\partial \mathbf{m}}{\partial y}) dx dy$ with \mathbf{m} being the reduced magnetization, their static and dynamic properties depend on their own internal structures [8, 12].

The most important internal degree of freedom of particle-like topological spin textures is their helicity [8, 12, 27, 28]. For example, among the magnetic quasiparticle family, the skyrmion is an exemplary member that can be found in ultrathin magnetic layers and low-dimensional magnets [3–12, 29–31], of which the helicity is mainly determined by the type of DM interactions [8, 16]. It shows Néel-type helicity in magnetic layers with interface-induced DM interactions [13–15], and shows Bloch-type helicity in magnets with bulk DM interactions (Fig. 1) [29–31]. For either case, the helicity structure of a skyrmion is centrosymmetric with respect to the skyrmion center. The existence of skyrmions with helicity asymmetry as well as their static and dynamic properties have remained unexplored.

In nanoscience, Janus particles [Fig. 1(a)] are a special type of highly functional particles named after the god Janus [Fig. 1(b)], which have at least two surfaces showing different or asymmetric physical properties [32, 33]. They can be fabricated at nanoscale and microscale dimensions, and due to

their multifunctionalized surface structures, they play important roles in various fields, including soft matter, active matter, biomedical science, and electronics [32–37]. For example, catalytically active Janus particles with asymmetric reaction surfaces can demonstrate self-propulsion and thus, can be used for active matter experiments [38]. Also, magnetoactive Janus particles can be used to build a multifunctional swarm metamaterial system for programmable dynamic display, non-volatile memory, and information encryption [39].

The concept of Janus particles could be shifted to magnetic quasiparticles, which have at least two different or asymmetric internal physical structures. For example, skyrmions with asymmetric helicity structures may be treated as Janus quasiparticles in magnetic materials. Most recently, experimentalists have demonstrated the possibility to engineer the sign of DM interactions in magnetic layers [40, 41], which is an effective way to modify the internal structures of skyrmions and will be the key to realize Janus skyrmions.

In this work, we show that one may artificially construct a Janus skyrmion with unique helicity asymmetry at the engineered interface between two magnetic regions with different types and signs of DM interactions. We explore the dynamics of such a Janus skyrmion with $|Q| = 1$ driven by magnetic field, spin current, or thermal fluctuations. We find that the Janus skyrmion can be viewed as a hybridization of a Néel-type and Bloch-type skyrmions, but its mobility is limited by the one-dimensional interface, leading to exotic properties that cannot be found in Néel-type and Bloch-type skyrmions.

From Janus particle to Janus skyrmion.—We first study the static structure of a Janus skyrmion. A Janus particle has two faces with different properties [Fig. 1(a)], therefore, we focus on a Janus skyrmion with two different helicity structures, as illustrated in Figs. 1(c) and 1(d). The left half of

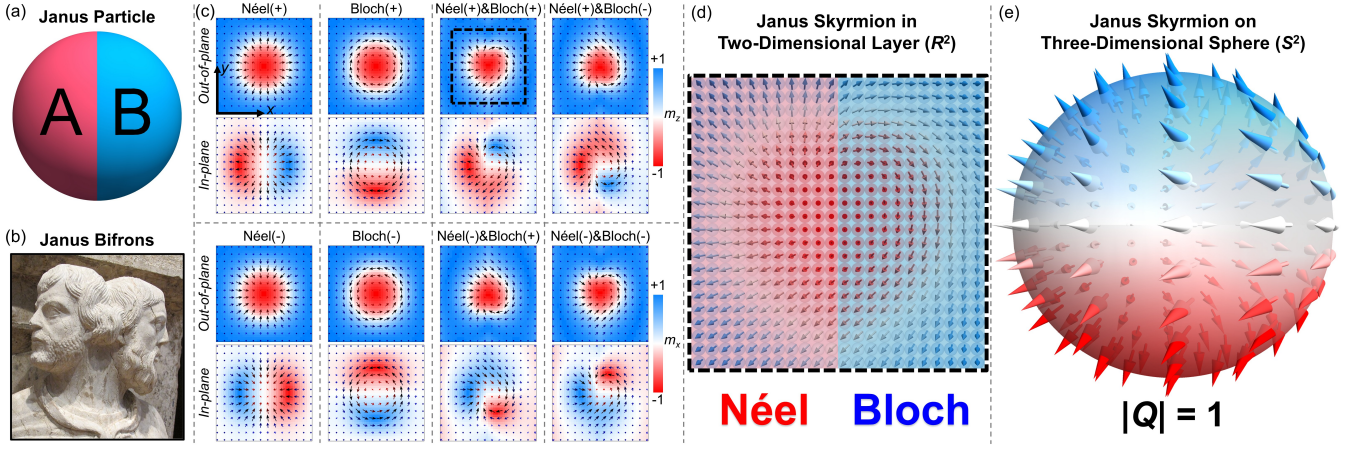


FIG. 1. Janus skyrmion quasiparticle with two-faced asymmetric helicity at the interface. (a) A basic Janus particle has two distinct surfaces, that is, the left side A and right side B, which show different or asymmetric properties. (b) The statue of the two-faced god Janus Bifrons, the ancient Roman god of beginnings and transitions, who is able to look at opposite directions. The image is a cropped version from wikipedia.org, licensed under the Creative Commons Attribution-Share Alike 3.0 Unported License (<https://creativecommons.org/licenses/by-sa/3.0>). (c) Top view of various relaxed Néel-type, Bloch-type, and Janus skyrmions with $Q = -1$. Skyrmions are fully relaxed at the center of a square magnetic layer with the same or two different types of DM interactions. The length, width, and thickness of the monolayer are equal to 40 nm, 40 nm, and 1 nm, respectively. The cell size is $1 \times 1 \times 1 \text{ nm}^3$. No external magnetic field is applied. For Néel-type and Bloch-type skyrmions, the DM interaction is uniform and of the same type in the model. For Janus skyrmions, the value of Néel-type DM interaction in the left region ($x = 0 - 20 \text{ nm}$) is fixed at $D_L = \pm 3.7 \text{ mJ m}^{-2}$, and the strength of Bloch-type DM interaction in the right region ($x = 20 - 40 \text{ nm}$) is set to $|D_R| = |D_L|$. The type and sign of D_L and D_R are indicated beyond each skyrmion configuration. Other default parameters are: $\alpha = 0.3$, $M_S = 580 \text{ kA m}^{-1}$, $A = 15 \text{ pJ m}^{-1}$, and $K = 0.8 \text{ MJ m}^{-3}$. The color scale represents the reduced out-of-plane (m_z) or in-plane (m_x) magnetization component. The magnetization configurations are indicated by black arrows. (d) A basic Janus skyrmion has two distinct helicity structures. For example, the left half is with Néel-type helicity, and the right half is with Bloch-type helicity. The shape of the Janus skyrmion is thus like a heart, which is in stark contrast to a normal skyrmion with centrosymmetric helicity. (e) Topological mapping of the spin configurations of a two-dimensional Janus skyrmion with $Q = -1$ [(d)] onto a three-dimensional 2-sphere.

the Janus skyrmion is of Néel-type helicity, while the right half is of Bloch-type helicity. Such a helicity structure is not centrosymmetric with respect to the skyrmion center, which is different to skyrmions with intermediate helicity between Néel-type and Bloch-type ones [42–46]. Consequently, the Janus skyrmion with helicity asymmetry has a unique heart-like shape but carries a topological charge carried of $|Q| = 1$.

We assume that a Janus skyrmion with $Q = -1$ and two different helicity structures is formed at the interface between two magnetic regions with different types of DM interactions. In our simulation [Fig. 1(c)], we place and relax a skyrmion at the center of a magnetic layer. The size of the magnetic layer is $40 \times 40 \times 1 \text{ nm}^3$, which includes 1,600 spins. The spin dynamics is governed by the Landau-Lifshitz-Gilbert (LLG) equation $\partial_t \mathbf{m} = -\gamma_0 \mathbf{m} \times \mathbf{h}_{\text{eff}} + \alpha(\mathbf{m} \times \partial_t \mathbf{m})$, which is solved by using the OOMMF simulator [47]. In the LLG equation, the absolute gyromagnetic ratio $\gamma_0 = 2.211 \times 10^5 \text{ m A}^{-1} \text{ s}^{-1}$ and the damping parameter $\alpha = 0.3$. The effective field $\mathbf{h}_{\text{eff}} = -\frac{1}{\mu_0 M_S} \cdot \frac{\delta \varepsilon}{\delta \mathbf{m}}$, where μ_0 and ε denote the vacuum permeability constant and average energy density, respectively. The average energy density includes the contributions from the ferromagnetic exchange interaction, DM exchange interactions (Néel-type and Bloch-type), perpendicular magnetic anisotropy (PMA), demagnetization, and applied magnetic field, given as $\varepsilon = A(\nabla \mathbf{m})^2 + D_N[m_z(\mathbf{m} \cdot \nabla) - (\nabla \cdot \mathbf{m})m_z] +$

$D_B[\mathbf{m} \cdot (\nabla \times \mathbf{m})] - K(\mathbf{n} \cdot \mathbf{m})^2 - \frac{M_S}{2}(\mathbf{m} \cdot \mathbf{B}_d) - M_S(\mathbf{m} \cdot \mathbf{B}_a)$. Note that D_N and D_B stand for the Néel-type and Bloch-type DM interaction parameters, respectively. \mathbf{B}_d is the demagnetization field, \mathbf{B}_a is the applied magnetic field, and \mathbf{n} is the unit surface normal vector. The default magnetic parameters are [16, 17]: the saturation magnetization $M_S = 580 \text{ kA m}^{-1}$, the exchange constant $A = 15 \text{ pJ m}^{-1}$, and PMA constant $K = 0.8 \text{ MJ m}^{-3}$.

As shown in Fig. 1(c), if we consider uniform Néel-type or Bloch-type DM interaction in the magnetic layer (either positive or negative), the relaxed skyrmion is of Néel-type or Bloch-type, where the helicity structure is centrosymmetric with respect to the skyrmion center. However, if we assume a Néel-type DM interaction in the left half of the magnetic layer ($x \in [0 \text{ nm}, 20 \text{ nm}]$), and a Bloch-type DM interaction in the right half of the magnetic layer ($x \in [20 \text{ nm}, 40 \text{ nm}]$), the relaxed skyrmion at the interface between the two different magnetic regions shows hybrid and asymmetric helicity structures, including both Néel-type and Bloch-type spin configurations. Such a Janus skyrmion is stable at the D_N - D_B interface and its topological charge is $Q = -1$ [Fig. 1(e)]. Its asymmetric internal spin configurations can be modified by changing the sign of DM interaction in each region [Fig. 1(c)]. In Supplementary Fig. 1 [48], we also show that the size and shape of the Janus skyrmion depend on the strength of the DM interaction in each region. The Janus skyrmion may be deformed

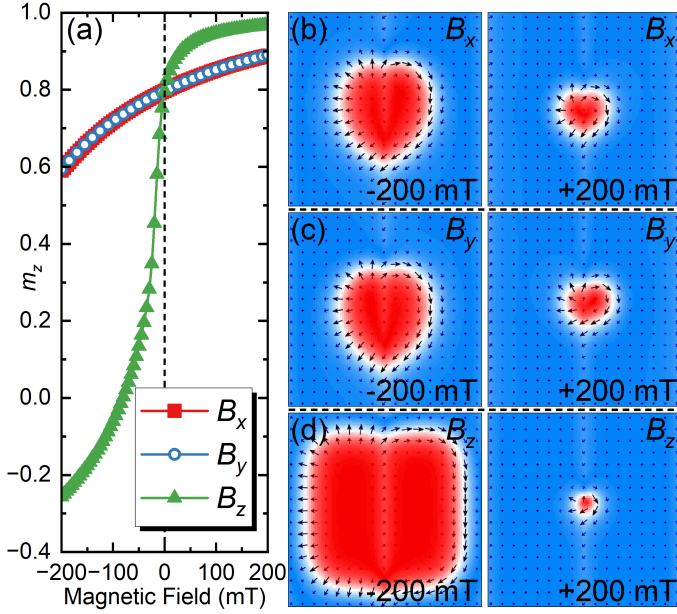


FIG. 2. Manipulation of a static Janus skyrmion by in-plane or out-of-plane magnetic field. (a) Reduced out-of-plane magnetization (m_z) of the model as functions of applied external magnetic fields. The magnetic field is applied in the x , y , or z direction, which scans from -200 mT to $+200$ mT. (b) Snapshots of the Janus skyrmion at $B_x = \pm 200$ mT. (c) Snapshots of the Janus skyrmion at $B_y = \pm 200$ mT. (d) Snapshots of the Janus skyrmion at $B_z = \pm 200$ mT. Here, the Janus skyrmion is stabilized at the interface between Néel-type (left) and Bloch-type (right) DM interactions. $D_L = D_R = 3.5$ mJ m $^{-2}$. The model size is $100 \times 100 \times 1$ nm 3 . Other parameters are given in Fig. 1 caption.

when the DM interactions in the left and right regions are not equal to each other.

In-plane and out-of-plane fields.—In Fig. 2, we apply an external magnetic field B_d to a Janus skyrmion, and observe its response to the field. The Janus skyrmion is initially relaxed in a magnetic layer of $100 \times 100 \times 1$ nm 3 , which includes 10,000 spins. The DM interaction in the left half of the magnetic layer is of Néel-type, and it is of Bloch-type in the right half. The relaxed Janus skyrmion at zero magnetic field shows asymmetric helicity, as given in Fig. 1(d).

In theory, a normal Néel-type or Bloch-type skyrmion [Fig. 1(c)] cannot be manipulated by a moderate in-plane magnetic field, as the magnetic field forces acting on the in-plane spins of the skyrmion will cancel with each other due to the centrosymmetry of the helicity structure. Only a strong in-plane magnetic field may deform the skyrmion into a non-circular shape by dragging perpendicularly magnetized spins into the x - y plane [49]. However, we find that the size of the Janus skyrmion with helicity asymmetry can be adjusted by an in-plane magnetic field. In Fig. 2, an external magnetic field applied in the $-x$ or $-y$ direction could increase the skyrmion size, while a field applied in the $+x$ or $+y$ direction could shrink the skyrmion. This is a unique feature that cannot be found in normal circular skyrmions with cen-

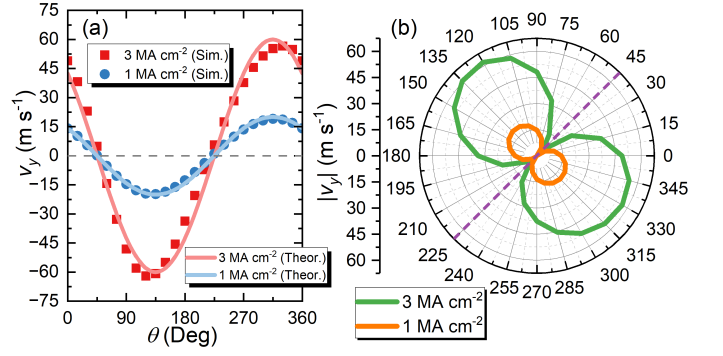


FIG. 3. Current-induced dynamics of a Janus skyrmion at the interface (θ dependence). (a) The velocity of the Janus skyrmion along the interface (i.e., $\pm y$ directions) as functions of the spin polarization angle (θ). Symbols are simulation results, and curves show theoretical solutions. (b) The θ -dependent speed of the Janus skyrmion moving along the interface. The driving current density j is fixed at 1 or 3 MA cm $^{-2}$. Only simulation results are shown. Here, the Janus skyrmion is stabilized at the interface between Néel-type (left) and Bloch-type (right) DM interactions. $D_L = D_R = 3.5$ mJ m $^{-2}$. The model size is $100 \times 100 \times 1$ nm 3 . Other parameters are given in Fig. 1 caption.

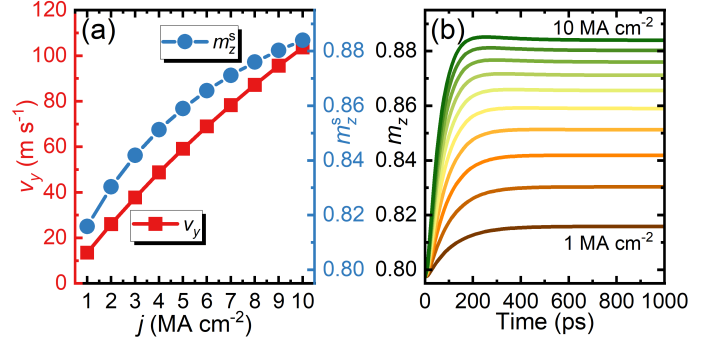


FIG. 4. Current-induced dynamics of a Janus skyrmion at the interface (j dependence). (a) Left: The velocity of the Janus skyrmion along the interface (i.e., $\pm y$ directions) as a function of the driving current density (j). Right: The reduced out-of-plane magnetization of the system obtained during the stable motion (m_z^s) as a function of j . The spin polarization angle is fixed at $\theta = 270$ degrees (i.e., $\mathbf{p} = -\hat{y}$). (b) The time-dependent m_z during the motion of a Janus skyrmion driven by different current densities ($j = 1 - 10$ MA cm $^{-2}$). See Fig. 3 caption for other parameters.

troscopic helicity structures. Indeed, similar to the case of a normal skyrmion, an out-of-plane magnetic field applied in the $\pm z$ direction can modify the size of the Janus skyrmion, which is an expected result.

Current-induced dynamics.—The Janus skyrmion is an interfacial state stabilized at the interface. Although it is a two-dimensional topological spin texture, its dynamics will be affected by the interface and should be largely different to that of a normal skyrmion. Here, we explore the dynamics of a Janus skyrmion at the interface driven by a vertical spin current [13–15]. Initially, a Janus skyrmion is relaxed at the center of a magnetic layer ($100 \times 100 \times 1$ nm 3) with periodic

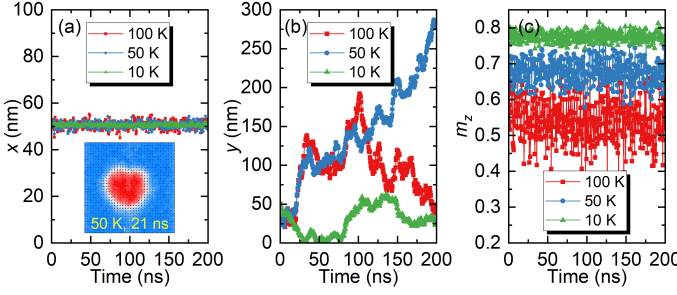


FIG. 5. One-dimensional Brownian random walk of a Janus skyrmion at the interface. (a) Time-dependent position of the Janus skyrmion in the x dimension. (b) Time-dependent position of the Janus skyrmion in the y dimension. (c) Time-dependent m_z of the model. Here, the Brownian dynamics of the Janus skyrmion is simulated at three different temperatures ($T = 10, 50$, and 100 K). See Fig. 3 caption for other parameters.

boundary conditions applied in both x and y directions. The DM interaction in the left half of the magnetic layer is of Néel-type, and it is of Bloch-type in the right half. We then apply a vertical spin current to drive the Janus skyrmion into motion, which can be realized by the spin Hall effect in the substrate underneath the magnetic layer [13–17].

To simulate current-induced dynamics, a damping-like spin Hall torque is included in the right-hand side of the LLG equation, given as $\tau_d = u(\mathbf{m} \times \mathbf{p} \times \mathbf{m})$. The coefficient $u = |(\gamma_0 \hbar / \mu_0 e)| \cdot (j \theta_{\text{SH}} / 2aM_S)$, where \hbar is the reduced Planck constant, e is the electron charge, a is the magnetic layer thickness, j is the current density, $\theta_{\text{SH}} = 1$ is the spin Hall angle, and \mathbf{p} is the spin polarization direction. The spin-polarization angle between \mathbf{p} and the $+x$ direction is defined as θ , which can be adjusted by tuning the in-plane electron flow direction in the substrate [16, 17].

In stark contrast to a normal skyrmion driven by the spin Hall torque, of which the velocity direction (i.e., skyrmion Hall angle) depends on θ but the speed is independent of θ , the current-induced dynamics of the Janus skyrmion is limited to a one-dimensional motion along the interface (i.e., $\pm y$ directions) without showing the skyrmion Hall effect. Both the speed and motion direction of the Janus depend on θ , as shown in Figs. 3(a) and 3(b) (Supplementary Videos 1 and 2 [48]). It can move toward the $+y$ or $-y$ direction, and its speed varies with θ for a given j .

As a larger j may lead to slight deformation of the Janus skyrmion, the $|v_y|$ - θ relation could be slightly asymmetric with respect to the θ axis corresponding to $|v_y| = 0$ [Fig. 3(b)]. When θ is fixed at a given value, for example, $\theta = 270$ degrees, the speed of the Janus skyrmion increases with increasing j and a larger j also leads to more obvious deformation of the Janus skyrmion [Fig. 4(a)], which can be seen from the time-dependent m_z during the current-induced motion [Fig. 4(b)] (Supplementary Video 3 [48]).

A normal skyrmion is usually repelled by magnetic surfaces and interfaces, while the Janus skyrmion is an interfacial state attracted by its hosting interface. Hence, the Janus

skyrmion can be viewed as a unique topological quasiparticle strictly confined in a one-dimensional potential well [50]. Its current-induced dynamics could be described by the Thiele equation [16, 17, 27, 51] with the assumption that an interface-induced force \mathbf{F}_x is acting on the Janus skyrmion and $v_x = 0$. The velocity solution is thus given as $v_y = c \cdot \cos(\theta + \pi/4)$ with $c = |\sqrt{2}u/2\alpha\mathcal{D}| \cdot \mathcal{I}$ being a constant determined by the driving force $u \sim j$ and the Janus skyrmion profile (Supplementary Note 1 [48]). Note that \mathcal{D} is the diagonal entries of the dissipative tensor in the Thiele equation and \mathcal{I} is related to the spin-torque efficiency over the skyrmion [16, 17, 27, 51]. In Fig. 3, it can be seen that the simulation results are in a good agreement with the theoretical velocity solutions, where $c = 20$ for $j = 1 \text{ MA cm}^{-2}$ and $c = 60$ for $j = 3 \text{ MA cm}^{-2}$. Note that a current-driven Janus skyrmion may be detached from the interface when \mathbf{F}_x is too strong (Supplementary Fig. 2 [48]), which then transforms into a normal skyrmion (Supplementary Videos 4 and 5 [48]). We also compare the current-induced motion of a Janus skyrmion with that of normal Néel-type and Bloch-type skyrmions in Supplementary Note 1 [48].

One-dimensional random walk.—As the Janus skyrmion can only move along the interface, it should be able to demonstrate one-dimensional random walk at the interface. To examine this prediction, we introduce a thermal fluctuation term into the LLG equation [52], and simulate the Brownian motion of a Janus skyrmion at finite temperature. The spin dynamics at finite temperature is governed by the stochastic LLG equation $\partial_t \mathbf{m} = -\gamma_0 \mathbf{m} \times (\mathbf{h}_{\text{eff}} + \mathbf{h}_f) + \alpha(\mathbf{m} \times \partial_t \mathbf{m})$, where \mathbf{h}_f is a thermal fluctuating field satisfying $\langle h_i(\mathbf{x}, t) \rangle = 0$ and $\langle h_i(\mathbf{x}, t) h_k(\mathbf{x}', t') \rangle = \frac{2\alpha k_B T}{M_S \gamma_0 \mu_0 V} \delta_{ik} \delta(\mathbf{x} - \mathbf{x}') \delta(t - t')$. i and k are Cartesian components, k_B is the Boltzmann constant, T is the temperature, and V is the volume of a single mesh cell. δ_{ik} and $\delta(\dots)$ denote the Kronecker and Dirac delta symbols, respectively. In all simulations, a fixed finite-temperature integration time step of 10 fs is applied.

In Fig. 5, it can be seen that the Janus skyrmion demonstrates obvious one-dimensional random walk along the interface (Supplementary Videos 6–8 [48]). The random walk diffusion in the y dimension increases with T [Fig. 5(b)], but the skyrmion position in the x dimension only slightly fluctuates with time [Fig. 5(a)]. The Janus skyrmion size also increases with T , which can be seen from time-dependent m_z in Fig. 5(c). The one-dimensional Brownian motion is a unique thermal dynamic feature of interfacial quasiparticles. A normal skyrmion usually demonstrates two-dimensional Brownian motion [53–61].

Conclusions.—We have explored the unique dynamics of a Janus skyrmion induced by magnetic field, spin current, or temperature. The Janus skyrmion is stabilized at the interface between two magnetic regions with different types of antisymmetric exchange interactions. Its helicity structure include both Néel-type and Bloch-type components. The dynamic behaviors of a Janus skyrmion largely differ from that of a normal skyrmion as it is topological quasiparticle stabilized and attached to the interface. The dynamic degree of

freedom of a Janus skyrmion is limited by the interface, and consequently, the speed of a Janus skyrmion moving along the interface could be controlled by the spin polarization angle, and it will not show the skyrmion Hall effect. Thermal fluctuations also lead to one-dimensional random walk of the Janus skyrmion at the interface, which is different to normal skyrmions that can diffuse in two dimensions. It is also found that both in-plane and out-of-plane magnetic fields can modify the size of a Janus skyrmion due to its helicity asymmetry. The size of normal skyrmions with symmetric helicity structures cannot be adjusted by an in-plane magnetic field. The asymmetric helicity structures of heart-shaped Janus skyrmions result in distinctive responses to magnetic field, spin current, and temperature. As the Janus skyrmion does not show the skyrmion Hall effect, it could be a promising building block for racetrack-type device applications [62–66]. This work will pave the way for the understanding of topological quasiparticles at material interfaces.

X.Z. and M.M. acknowledge support by the CREST, the Japan Science and Technology Agency (Grant No. JP-MJCR20T1). X.Z. also acknowledges support by the Grants-in-Aid for Scientific Research from JSPS KAKENHI (Grant No. JP25K17939 and No. JP20F20363). M.M. also acknowledges support by the Grants-in-Aid for Scientific Research from JSPS KAKENHI (Grants No. JP25H00611, No. JP24H02231, No. JP23H04522, and No. JP20H00337) and the Waseda University Grant for Special Research Projects (Grant No. 2025C-133). R.Z. acknowledges support by the State Key Laboratory of Displays and Opto-Electronics (Project Reference: ITC-PSKL12EG02). C.R. and C.J.O.R. acknowledge the support by the U.S. Department of Energy through the Los Alamos National Laboratory. Los Alamos National Laboratory is operated by Triad National Security, LLC, for the National Nuclear Security Administration of the U.S. Department of Energy (Contract No. 892333218NCA000001). Y.Z. acknowledges support by the Shenzhen Fundamental Research Fund (Grant No. JCYJ20210324120213037), the National Natural Science Foundation of China (12374123), the Guangdong Basic Research Center of Excellence for Aggregate Science, and the 2023 SZSTI Stable Support Scheme.

* Email: xichaozhang@aoni.waseda.jp

† Email: masa_mochizuki@waseda.jp

- [1] I. Dzyaloshinsky, *J. Phys. Chem. Solids* **4**, 241 (1958).
- [2] T. Moriya, *Phys. Rev.* **120**, 91 (1960).
- [3] M. Mochizuki and S. Seki, *J. Phys.: Condens. Matter* **27**, 503001 (2015).
- [4] G. Finocchio, F. Büttner, R. Tomasello, M. Carpentieri, and M. Kläui, *J. Phys. D: Appl. Phys.* **49**, 423001 (2016).
- [5] R. Wiesendanger, *Nat. Rev. Mat.* **1**, 16044 (2016).
- [6] A. Fert, N. Reyren, and V. Cros, *Nat. Rev. Mater.* **2**, 17031 (2017).
- [7] W. Jiang, G. Chen, K. Liu, J. Zang, S. G. Velthuis, and A. Hoffmann, *Phys. Rep.* **704**, 1 (2017).
- [8] X. Zhang, Y. Zhou, K. M. Song, T.-E. Park, J. Xia, M. Ezawa, X. Liu, W. Zhao, G. Zhao, and S. Woo, *J. Phys. Condens. Matter* **32**, 143001 (2020).
- [9] B. Göbel, I. Mertig, and O. A. Tretiakov, *Phys. Rep.* **895**, 1 (2021).
- [10] N. Del-Valle, J. Castell-Queralt, L. González-Gómez, and C. Navau, *APL Mater.* **10**, 010702 (2022).
- [11] C. Reichhardt, C. J. O. Reichhardt, and M. V. Milosevic, *Rev. Mod. Phys.* **94**, 035005 (2022).
- [12] Y. Ohki and M. Mochizuki, *J. Phys.: Condens. Matter* **37**, 023003 (2024).
- [13] W. Jiang, P. Upadhyaya, W. Zhang, G. Yu, M. B. Jungfleisch, F. Y. Fradin, J. E. Pearson, Y. Tserkovnyak, K. L. Wang, O. Heinonen, S. G. E. te Velthuis, and A. Hoffmann, *Science* **349**, 283 (2015).
- [14] W. Jiang, X. Zhang, G. Yu, W. Zhang, X. Wang, M. Benjamin Jungfleisch, J. E. Pearson, X. Cheng, O. Heinonen, K. L. Wang, Y. Zhou, A. Hoffmann, and S. G. E. Velthuis, *Nat. Phys.* **13**, 162 (2017).
- [15] K. Litzius, I. Lemesch, B. Kruger, P. Bassirian, L. Caretta, K. Richter, F. Büttner, K. Sato, O. A. Tretiakov, J. Forster, R. M. Reeve, M. Weigand, I. Bykova, H. Stoll, G. Schutz, G. S. D. Beach, and M. Kläui, *Nat. Phys.* **13**, 170 (2017).
- [16] R. Tomasello, E. Martinez, R. Zivieri, L. Torres, M. Carpentieri, and G. Finocchio, *Sci. Rep.* **4**, 6784 (2014).
- [17] X. Zhang, J. Xia, O. A. Tretiakov, M. Ezawa, G. Zhao, Y. Zhou, X. Liu, and M. Mochizuki, *Phys. Rev. B* **108**, 144428 (2023).
- [18] K. Raab, M. Schmitt, M. A. Brems, J. Rothorl, F. Kammerbauer, S. Krishnia, M. Kläui, and P. Virnau, *Phys. Rev. E* **110**, L042601 (2024).
- [19] W. Kang, Y. Huang, X. Zhang, Y. Zhou, and W. Zhao, *Proc. IEEE* **104**, 2040 (2016).
- [20] S. Li, W. Kang, X. Zhang, T. Nie, Y. Zhou, K. L. Wang, and W. Zhao, *Mater. Horiz.* **8**, 854 (2021).
- [21] S. Luo and L. You, *APL Mater.* **9**, 050901 (2021).
- [22] C. H. Marrows and K. Zeissler, *Appl. Phys. Lett.* **119**, 250502 (2021).
- [23] V. Lohani, C. Hickey, J. Masell, and A. Rosch, *Phys. Rev. X* **9**, 041063 (2019).
- [24] C. Psaroudaki and C. Panagopoulos, *Phys. Rev. Lett.* **127**, 067201 (2021).
- [25] C. Psaroudaki and C. Panagopoulos, *Phys. Rev. B* **106**, 104422 (2022).
- [26] J. Xia, X. Zhang, X. Liu, Y. Zhou, and M. Ezawa, *Phys. Rev. Lett.* **130**, 106701 (2023).
- [27] X. Zhang, J. Xia, Y. Zhou, X. Liu, H. Zhang, and M. Ezawa, *Nat. Commun.* **8**, 1717 (2017).
- [28] X. Zhang, J. Xia, O. A. Tretiakov, H. T. Diep, G. Zhao, J. Yang, Y. Zhou, M. Ezawa, and X. Liu, *J. Magn. Soc. Jpn.* **47**, 20 (2023).
- [29] U. K. Röbler, A. N. Bogdanov, and C. Pfleiderer, *Nature* **442**, 797 (2006).
- [30] S. Mühlbauer, B. Binz, F. Jonietz, C. Pfleiderer, A. Rosch, A. Neubauer, R. Georgii, and P. Böni, *Science* **323**, 915 (2009).
- [31] X. Z. Yu, Y. Onose, N. Kanazawa, J. H. Park, J. H. Han, Y. Matsui, N. Nagaosa, and Y. Tokura, *Nature* **465**, 901 (2010).
- [32] A. Walther and A. H. E. Müller, *Soft Matter* **4**, 663 (2008).
- [33] A. Walther and A. H. E. Müller, *Chem. Rev.* **113**, 5194 (2013).
- [34] F. Li, D. P. Josephson, and A. Stein, *Angew. Chem. Int. Ed.* **50**, 360 (2011).
- [35] J. Zhang, B. A. Grzybowski, and S. Granick, *Langmuir* **33**, 6964 (2017).
- [36] H. Su, C. A. Hurd Price, L. Jing, Q. Tian, J. Liu, and K. Qian, *Mater. Today Bio* **4**, 100033 (2019).

- [37] R. Zhang, A. Mozaffari, and J. J. de Pablo, *Nat. Rev. Mater.* **6**, 437 (2021).
- [38] W. F. Paxton, K. C. Kistler, C. C. Olmeda, A. Sen, S. K. Angelo, Y. Cao, T. E. Mallouk, P. E. Lammert, and V. H. Crespi, *J. Am. Chem. Soc.* **126**, 13424 (2004).
- [39] Z. Zhang, J. E. Raymond, J. Lahann, and A. Pena-Francesch, *Adv. Mater.* **36**, 2406149 (2024).
- [40] H. Niu, H. G. Yoon, H. Y. Kwon, Z. Cheng, S. Fu, H. Zhu, B. Miao, L. Sun, Y. Wu, A. K. Schmid, K. Liu, C. Won, H. Ding, and G. Chen, *Nat. Commun.* **16**, 3453 (2025).
- [41] H. Niu, H. Y. Kwon, T. Ma, Z. Cheng, C. Ophus, B. Miao, L. Sun, Y. Wu, K. Liu, S. S. P. Parkin, C. Won, A. K. Schmid, H. Ding, and G. Chen, *Nat. Commun.* **15**, 10199 (2024).
- [42] K.-W. Kim, K.-W. Moon, N. Kerber, J. Nothhelfer, and K. Everschor-Sitte, *Phys. Rev. B* **97**, 224427 (2018).
- [43] B. Dai, D. Wu, S. A. Razavi, S. Xu, H. He, Q. Shu, M. Jackson, F. Mahfouzi, H. Huang, Q. Pan, Y. Cheng, T. Qu, T. Wang, L. Tai, K. Wong, N. Kioussis, K. L. Wang, *Sci. Adv.* **9**, eade6836 (2023).
- [44] L. Kong, J. Tang, Y. Wu, W. Wang, J. Jiang, Y. Wang, J. Li, Y. Xiong, and S. Wang, *Phys. Rev. B* **109**, 014401 (2024).
- [45] Y. Liu, B. Yang, X. Guo, S. Picozzi, and Y. Yan, *Phys. Rev. B* **109**, 094431 (2024).
- [46] M. P. M. Akhri, E. Suprayoga, and A. B. Cahaya, *J. Phys. D: Appl. Phys.* **57**, 165303 (2024).
- [47] M. J. Donahue and D. G. Porter, Interagency Report No. NISTIR 6376 (National Institute of Standards and Technology, Gaithersburg, MD, 1999).
- [48] See Supplemental Material at [\[URL\]](#) for supplementary note (Thiele equation), supplementary figures, and supplemental videos showing the current-induced and temperature-induced dynamics of a Janus skyrmion.
- [49] S.-Z. Lin and A. Saxena, *Phys. Rev. B* **92**, 180401(R) (2015).
- [50] C. Reichhardt and C. J. Olson Reichhardt, *Phys. Rev. B* **94**, 094413 (2016).
- [51] A. A. Thiele, *Phys. Rev. Lett.* **30**, 230 (1973).
- [52] A. Vansteenkiste, J. Leliaert, M. Dvornik, M. Helsen, F. Garcia-Sanchez, and B. V. Waeyenberge, *AIP Adv.* **4**, 107133 (2014).
- [53] J. Barker and O. A. Tretiakov, *Phys. Rev. Lett.* **116**, 147203 (2016).
- [54] J. Miltat, S. Rohart, and A. Thiaville, *Phys. Rev. B* **97**, 214426 (2018).
- [55] T. Nozaki, Y. Jibiki, M. Goto, E. Tamura, T. Nozaki, H. Kubota, A. Fukushima, S. Yuasa, and Y. Suzuki, *Appl. Phys. Lett.* **114**, 012402 (2019).
- [56] L. Zhao, Z. Wang, X. Zhang, X. Liang, J. Xia, K. Wu, H. A. Zhou, Y. Dong, G. Yu, K. L. Wang, X. Liu, Y. Zhou, and W. Jiang, *Phys. Rev. Lett.* **125**, 027206 (2020).
- [57] K. Y. Jing, C. Wang, and X. R. Wang, *Phys. Rev. B* **103**, 174430 (2021).
- [58] Y. Zhou, R. Mansell, T. Ala-Nissila, and S. van Dijken, *Phys. Rev. B* **104**, 144417 (2021).
- [59] S. Miki, Y. Jibiki, E. Tamura, M. Goto, M. Oogane, J. Cho, R. Ishikawa, H. Nomura, and Y. Suzuki, *J. Phys. Soc. Jpn.* **90**, 083601 (2021).
- [60] X. Zhang, J. Xia, O. A. Tretiakov, M. Ezawa, G. Zhao, Y. Zhou, X. Liu, and M. Mochizuki, *Nano Lett.* **23**, 11793 (2023).
- [61] X. Zhang, C. Reichhardt, C. J. O. Reichhardt, Y. Zhou, Y. Xu, and M. Mochizuki, *arXiv:2506.14090* (2025).
- [62] S. S. P. Parkin, M. Hayashi, and L. Thomas, *Science* **320**, 190 (2008).
- [63] S. Parkin and S.-H. Yang, *Nat. Nanotechnol.* **10**, 195 (2015).
- [64] K. Gu, Y. Guan, B. K. Hazra, H. Deniz, A. Migliorini, W. Zhang, and S. S. P. Parkin, *Nat. Nanotechnol.* **17**, 1065 (2022).
- [65] B. He, R. Tomasello, X. Luo, R. Zhang, Z. Nie, M. Carpentieri, X. Han, G. Finocchio, and Guoqiang Yu, *Nano Lett.* **23**, 9482 (2023).
- [66] B. W. Walker, C. Cui, F. Garcia-Sanchez, J. A. C. Incorvia, X. Hu, and J. S. Friedman, *Appl. Phys. Lett.* **118**, 192404 (2021).